University of Kent

Kent Academic Repository

Young, Paul and Callaghan, Peter (2026) *Design of Dual-Beam Reflectarrays and RIS Using a Sawtooth Phase Variation*. IEEE Antennas and Wireless Propagation Letters, 25 (5). pp. 2065-2069. ISSN 1536-1225.

Downloaded from
https://kar.kent.ac.uk/114578/ The University of Kent's Academic Repository KAR

The version of record is available from
https://doi.org/10.1109/LAWP.2026.3670955

This document version
Author's Accepted Manuscript

DOI for this version

Licence for this version
CC BY (Attribution)

Additional information
For the purpose of open access, the author(s) has applied a Creative Commons Attribution (CC BY) licence to any Author Accepted Manuscript version arising.

Versions of research works

Versions of Record
If this version is the version of record, it is the same as the published version available on the publisher's web site. Cite as the published version.

Author Accepted Manuscripts
If this document is identified as the Author Accepted Manuscript it is the version after peer review but before type setting, copy editing or publisher branding. Cite as Surname, Initial. (Year) 'Title of article'. To be published in ***Title of Journal*** , Volume and issue numbers [peer-reviewed accepted version]. Available at: DOI or URL (Accessed: date).

Enquiries
If you have questions about this document contact ResearchSupport@kent.ac.uk. Please include the URL of the record in KAR. If you believe that your, or a third party's rights have been compromised through this document please see our Take Down policy (available from https://www.kent.ac.uk/guides/kar-the-kent-academic-repository#policies).

AWPL-01-26-0064

Design of dual beam Reflectarrays and RIS using a sawtooth phase variation

Paul R. Young and Peter Callaghan

***Abstract*— A sawtooth phase function is proposed to assist in the design of dual beam reflectarray antennas and reconfigurable intelligent surfaces (RIS). By using Fourier analysis, simple design equations have been determined for the calculation of element phases for both wanted beam directions and beam amplitudes. A reflectarray surface with beams at +20° and -40° and relative beam amplitudes of 0 dB and -5 dB is investigated. Measurement and simulations from CST agree well with the design theory.**

***Index Terms*— Reflectarrays, metasurfaces, passive repeater, beam steering, reconfigurable intelligent surfaces**

I. INTRODUCTION

REFLECTARRAY SURFACES (RAS) form the basis of reflectarray antennas (RA) [1], replacing a curved reflector with a simple flat design. One area of growing interest is in the design of multi-beam antennas generating more than one beam. Basic design approaches use 'direct design' methods of geometrical aperture sharing (physically separate reflectors) or by superposition (SP) of aperture fields. Direct design methods have been shown to have significant limitations [2]. Superposition of fields can be accurate but requires both magnitude and phase so cannot be represented by a RAS with phase only, except for in a few special cases [3]. The usual approach requires 'indirect' design methods based on numerical optimization techniques. These can provide accurate patterns with an example of a quad beam pattern in [4] generated by a particle swarm optimizer (PSO). More recently optimization techniques [5] have been developed further for contoured beam RA using machine learning techniques based upon a 'unit cell' approximation. For faster computation the use of 'digital twins' has been proposed [6].

In recent years an emphasis has been placed on increasing channel capacity for 5G/6G services by use of dual-beam antenna designs. This may be achieved using physically separate beams, using frequency [7], hybrid designs integrating a reflectarray onto the surface of an active array [8], controlling left-hand and right-hand phases independently in circularly polarized antennas [9-11], multi-mode transmittarray elements [12] and hybrid transmittarray/ reflectarrays [13].

From a system point of view, channel capacity can also be increased by the use of RAS [18] acting as a passive 'smart skins' (SS) or, using electronic control, as reconfigurable intelligent surfaces (RIS) [14][15]. The optimization techniques of [5, 6] have been used for the design of smart skins producing dual beam and shaped beams [16-17]. For real-time operation of an RIS rapid calculation of the element phases will be needed [18] to achieve switching times below the transmission time intervals (TTIs) (1 ms for modern systems but future systems looking for less than 100 μs). As such a closed form expression (CFE) is needed (e.g. [19] used to create a flat-topped beam). Current research suggests using 1-bit or 2-bit digital RIS that may not model the CFE and then a 'look-up' table of elements will need to be created [18]. In this respect, the CFE can provide a better starting point.

Using the optimization approach to synthesize phases for a dual-beam linear array, the authors noticed the optimized values closely resembled a sawtooth function impressed on the nominal linear phase slope. As such, use of a sawtooth function as a closed form expression to design dual beam RAS is investigated here. In Section II we demonstrate the potential of a sawtooth phase function by comparison against the superposition approach. In section III Fourier analysis is used to derive some simple design equations that would suit rapid calculations for RIS. Section IV summarizes with the practical design of a RAS to evaluate the performance of a dual-beam pattern generated by this sawtooth phase function.

II. DUAL BEAMS GENERATED BY A SAWTOOTH PHASE

It is well known [20] that the co-polarized far field pattern, in the *x-z* plane, from a linearly polarized aperture in the *x-y* plane is given by

$$F(u) = \int_{-\infty}^{\infty} f(X) e^{j 2\pi u X} dX \qquad (1)$$

where $f(X)$ is the field in the aperture, assumed to vary only in the *x*-direction. The normalized distance is $X = x/\lambda$ and u is related to the angle in the *x-z* plane, θ, by $u = \sin(\theta)$. For the superposition (SP) approach [1] two waves, travelling at angles θ_0 and θ_1 are assumed, resulting in a magnitude and phase variation $f(X)$ across the aperture with the far field pattern determined from equation (1). An example of this is shown in Fig. 1 where a 99 mm wide aperture operating at 28 GHz is shown generating dual beams at $\theta_0 = 30°$ and $\theta_1 = -55°$ with the beam at θ_1 being 5 dB lower than that at θ_0, with the

Manuscript submitted dayth Month 2026

P. R. Young is with the School of Engineering, University of Kent, Kent, UK CT2 7NT. (phone +44 (0) 1227 823290 e-mail: P.R.Young@kent.ac.uk)

P. Callaghan is with the School of Engineering, University of Kent, Kent, UK CT2 7NT (e-mail: pc395@kent.ac.uk).

Color versions of one or more of the figures in this article are available online at http://ieeexplore.ieee.org

total energy normalized to unity. The beams are formed in the same plane as the aperture, i.e. beam steering in a single plane (linear array). (Note this can readily be transformed to beams in arbitrary directions by applying suitable geometric transformations, that is tilt the plane containing the beams with respect to the XOZ and then rotate around the z-axis). Since different amplitudes are required for the two beams both magnitude and phase variation are needed across the aperture, SP(ϕ) and SP(mag) in Fig 1(a). For reflectarray antennas and RIS only phase variation can be used and therefore this approach is not valid. If only the phase of the SP approach is used, with the magnitude set to 1, then the beam directions are maintained but there is a significant difference in the relative lobe amplitudes, see Fig 1(b). Phases can be found using numerical optimization that compensate for the lack of field magnitude variation required by a reflectarray design. Such optimized phases can be approximated as a linear phase slope (i.e. main beam at 30°) with a secondary sawtooth function imposed (i.e. second beam at -55°). This sawtooth phase function (Saw(ϕ)) is plotted in Fig. 1(a) - together with the nominal linear phase slope. The resulting pattern agrees well with the wanted patterns. For interest, the sawtooth phase is also plotted for a phase range of -180° to 180° to compare to the SP phase, illustrating the non-linearity in the SP phase to compensate for the magnitude variation.

III. Fourier Analysis for a Sawtooth Phase Function

In this section the analytical solution of equation (1) is given for the sawtooth phase function resulting in simple design formula for both the amplitude and direction of both beams. The analysis begins by finding the Fourier series representation of a continuously periodic sawtooth phase function, $\phi(X)$, as illustrated in Fig. 2(a). Here the phase has a peak variation, Φ_s, and a normalized period, X_s. From Fig 2(a), the periodic phase function is $\phi(X) = (\Phi_s/X_s)X$ for $|X| < X_s/2$, and hence the field in the aperture is

$$f(X + nX_s) = f(X) = e^{j\phi(X)} \tag{2}$$

for integer n. The complex Fourier series of (2) is given by

$$f(X) = \sum_{n=-\infty}^{\infty} C_n e^{j2n\pi X/X_s} \tag{3}$$

where

$$C_n = \operatorname{sinc}\left(\frac{\Phi_s - 2n\pi}{2}\right) \tag{4}$$

By adding a continuous linear phase of slope $-k_0 \sin\theta_0$ to the periodic phase function, equations (1), (3) and (4) yield

$$\begin{aligned} F_1(u) &= \sum_{n=-\infty}^{\infty} \int_{-\infty}^{\infty} C_n e^{j2\pi\left(u - \sin\theta_0 + \frac{n}{X_s}\right)X} dX \\ &= \sum_{n=-\infty}^{\infty} C_n \delta(u - \sin\theta_0 + n/Xs) \end{aligned} \tag{5}$$

where θ_0 is the required direction of the main beam and $\delta(x)$ is the Dirac delta function. Use of the shift property of the Fourier transform [21] has been used in deriving (5).

Equation (5) represents waves of amplitude C_n in directions $u = \sin\theta_0 - n/X_s$ (where only values for $|u| < 1$ are in real space). We see from (5) that the direction of the beams are controlled by the period, X_s, of the sawtooth phase function (together with the continuous linear phase slope) and from (4) the amplitude is controlled by the maximum phase variation, Φ_s. The values of C_n are plotted as a function of Φ_s, in Fig. 2(b). As Φ_s, increases, the amplitude of C_0 decreases, with the other Fourier harmonics increasing. These Fourier harmonics relate to beams in different directions. For $0 < \Phi_s < 2\pi$, only the first Fourier harmonic, C_1, has a magnitude comparable to C_0. Therefore, by carefully choosing Φ_s, the relative magnitude of this first harmonic can be controlled, resulting in a second beam. If we define A_s as the ratio of the first to main beam amplitude, $A_s = C_1/C_0$, then using (4) gives:

$$\Phi_s = \frac{2\pi A_s}{1 + A_s} \tag{6}$$

This allows the relative amplitude of the secondary to the main beam to be set by calculating Φ_s, for a required A_s. The other Fourier harmonics will also contribute to the pattern but are mostly much lower amplitudes and/or not in real space. However, as is seen in section IV these harmonics may end up as unwanted sidelobes when the surface is implemented as a periodic array of elements. The directions of the two beams are at θ_0 (main beam) for $n = 0$ and at θ_1 (secondary beam), for $n = 1$ where $u = \sin\theta_1 = \sin\theta_0 - 1/X_s$. Hence, X_s can be calculated from:

$$X_s = \left(\sin\theta_0 - \sin\theta_1\right)^{-1} \tag{7}$$

Equations (6) and (7), together with the linear phase, give control over the directions and relative magnitudes of the two beams, allowing a very simple design procedure to be followed. In a practical implementation, the surface will be finite, with a normalized width D. Including this with the phase function of (1) (*i.e.* limiting the integral to $\pm D/2$) and using [21] leads to:

$$F_2(u) = D\sum_{n=-\infty}^{\infty} C_n \operatorname{sinc}\left(\pi D(u - \sin\theta_0 + n/Xs)\right) \tag{8}$$

$F_2(u)$ is the pattern for an aperture with a continuous phase variation. For implementation by a reflectarray surface the phase is synthesized by an array of N elements spaced by a normalized distance d/λ where $D = Nd/\lambda$. This can be modelled using a sampling function represented by a Dirac comb with spacings of $X = md/\lambda$. This has a Fourier transform:

$$F_d(u) = \frac{\lambda}{d}\sum_{m=-\infty}^{\infty} A^m \delta\left(u - \frac{m\lambda}{d}\right) \tag{9}$$

where

$$A = \begin{cases} -1 & \text{for } N \text{ even} \\ 1 & \text{for } N \text{ odd} \end{cases}$$

The A^m term is required since for even N the array elements are offset by $d/(2\lambda)$. Convolving equation (8) and (9) gives the field for a finite sized reflectarray having a sawtooth phase function:

$$F_3(u) = \frac{D\lambda}{d}\sum_{n=-\infty}^{\infty}\sum_{m=-\infty}^{\infty} C_n A^m \operatorname{sinc}\left(\pi D\left(u - \sin\theta_0 + \frac{n}{X_s} + \frac{m\lambda}{d}\right)\right) \tag{10}$$

IV. APPLICATION OF SAWTOOTH PHASE IN REFLECTARRAY SURFACE DESIGN

The applicability of this sawtooth phase function is investigated by a practical design. A 99 mm by 99 mm RAS is to provide dual beams at $\theta_0 = 20°$ and $\theta_1 = -40°$ at 28 GHz, assuming a normally incident plane wave. For illustration, two designs are considered with the beam amplitude ratios, A_s, at 0 dB and -5 dB. An element spacing of 4.5 mm was chosen, to be less than $\lambda/2$. The nominal phase slope is 51.7° per element (for $\theta_0 = 20°$), with a sawtooth period, $x_s = \lambda X_s$, of 10.84 mm from (7) to achieve the second beam angle. From (6) the sawtooth peak phases, Φ_s, are π for $A_s = 0$ dB and 0.83π for $A_s = -5$ dB. For illustration these values are highlighted in Fig. 2(b), indicating the actual values for C_1 and C_0.

The resulting pattern for this sawtooth function design is complex, but as $F_3(u)$ is equivalent to calculating (1) using phases from (6) and (7), essentially the 'Array Factor' (AF), it is informative to plot (10) in stages as shown in Fig. 3. Inspection of (10) shows $F_3(u)$ is constructed by a set of continuous phase spectra, i.e. $F_2(u)$ of equation (8) offset by the 'sampling' period $m\lambda/d$. In Fig. 3 the terms in the series over m, for values of $m = -1$, 0 and +1, have been plotted in conjunction with the combined spectrum, $F_3(u)$. Fig. 3(b), where $m = 0$, is in fact the pattern that would be generated if there was a continuous phase variation across the aperture. From the Fourier series, a number of 'harmonics' generate beams at corresponding directions in u. Only two of these appear in visible space ($|u|<1$), the two desired beams at $\theta_0 = 20°$ and $\theta_1 = -40°$. From equation (10) it is possible for other harmonics to fall inside visible space depending upon the value of Φ_s. Although the amplitude of these terms (from equation 4) will be low, and may be acceptable. However, for the RAS design, formed from an array of elements, additional terms are generated by the 'sampling' process, such that higher order lobes can now be shifted into real-space as indicated in Fig. 3. The arrows trace lobes in $m = -1$ and $m = 1$ that contribute to the complete pattern $F_3(u)$. These shifted lobes may or may not increase the sidelobe levels, depending on how they combine.

To confirm the results experimental RAS were manufactured using a 'Phoenix' printed element [22] as illustrated in Fig. 4. For this arrangement the pattern is formed in the *x-z* plane. For a low-cost design a sandwich structure, Fig. 4(c), has been used. This has, potentially, half the cost of a solid PTFE based microwave substrate as in [19]. Here the elements were etched onto dielectric D1 (0.125 mm GTS5500 polyester film with $\varepsilon_r = 2.8$ and $\tan\delta = 0.008$), spaced from a metallic ground plane by spacer D3 (3 mm Rohacell 51HF Foam with $\varepsilon_r = 1.067$ and $\tan\delta = 0.0041$). To bond the structure, two layers of 3M 9088-200 0.2 mm thickness double coated acrylic tape ($\varepsilon_r \sim 3.0$ and $\tan\delta \sim 0.02$) were used (D2 & D4). Fig. 4(a) illustrates the complete RAS, with the details of the Phoenix element in Fig. 4(b). The element length L_r is adjusted to give the required phase with the two different designs compared in Fig. 4(d). It is seen only very subtle differences lead to the 5 dB difference in the relative beam amplitudes.

The designs were simulated in CST MWS and prototypes measured in the lab (using the same method as in [19,23]). The pattern, $F_3(u)$, does not include the effect of the element factor. By multiplying equation (10) by an element factor (EF) of $\cos^{1/2}\theta$ (suggested by [24]) close agreement between equation (10) and CST is seen in Fig. 5 for the A_s=-5 dB design. For comparison the bistatic radar cross section (BRCS) pattern achieved using MATLAB's PSO is included in Fig. 5, demonstrating that the sidelobes may be reduced further, although not meeting the design template (spec) 100%. However, the PSO calculation of the phases took 58 s compared to 16 μs using (2), demonstrating the potential for real-time calculation in RIS applications. The measured patterns compare well to CST in Fig. 5. Overall, there is good agreement, even with much of the sidelobe details.

The element factor impacts the amplitudes of each peak separately such that, for a desired beam ratio, A_s, the design value in (6) has to be corrected. To illustrate, simulations are presented in Fig. 6 for a design having $A_s = -3$dB, $\theta_0 = 30°$ with varying θ_1 from -70° to +70°. Using CST and the AF, the calculated peak values for the fixed beam, $\theta_0 = 30°$, and the ratio of the two beam amplitudes, A_s, are plotted against θ_1. Note for $\theta_1 = 30°$ there is a single beam having a peak of -1.3 dBm^2, not 0 dB, due to the EF. As θ_1 increases in value the peak of the θ_0 beam needs to be reduced to compensate for the EF effect. This indicates limited applicability for $\theta_1 > 60°$, as expected for broadside arrays. However, this maintains the A_s, plotted in Fig. 6, to within 1 dB. Again, simulations from CST agree well with the AF.

V. CONCLUSION

Use of a sawtooth phase function has provided simple closed form expressions for the design of a dual-beam reflectarray surfaces. Such calculations may lead to real-time beam steering desired in systems such as RIS. Fourier analysis also explains the generation of unwanted sidelobes that may be a limitation in this approach.

ACKNOWLEDGMENT

The authors thank Antonio Mendoza Mendoza for his valued support in the experimental work

REFERENCES

[1] P. Nayeri, F. Yang, and A. Z. Elsherbeni, "Multi-Beam and Shaped-Beam Reflectarray Antennas" in Reflectarray Antennas: Theory, Designs, and Applications, Wiley-IEEE Press. Online, 2018.

[2] J. Huang and J. A. Encinar, "Multi - beam reflectarrays" in Reflectarray Antennas. Piscataway, NJ, USA: IEEE Press, John Wiley & Sons, 2008.

[3] P. Nayeri, F. Yang and A. Z. Elsherbeni, "Design and Experiment of a Single-Feed Quad-Beam Reflectarray Antenna," in IEEE Trans, on Antennas and Propag., vol. 60, no. 2, pp. 1166-1171, Feb. 2012, doi:

[4] P. Nayeri, F. Yang, and A. Z. Elsherbeni, "Design of single-feed reflectarrays with asymmetric multi-beams," Proceedings of the 2012 IEEE International Symposium on Antennas and Propagation, Chicago, IL, USA, 2012, pp. 1-2, doi:

[5] D. R. Prado, J. A. López-Fernández, M. Arrebola, M. R. Pino, and G. Goussetis: "General framework for the efficient optimization of reflectarray antennas for contoured beam space applications" IEEE Access, vol. 6, pp. 72 295–72 310, 2018

[6] G. Oliveri, M. Salucci, and A. Massa, "Towards Efficient Reflectarray Digital Twins - An EM-Driven Machine Learning Perspective," IEEE

Trans. Antenn. Propag., vol. 70, no. 7, pp. 5078–5093, Jul. 2022., doi: 10.1109/TAP.2022.3155204

[7] Z. H. Jiang, Y. Zhang, and W. Hong, “Anisotropic Impedance Surface-Enabled Low-Profile Broadband Dual- Circularly Polarized Multibeam Reflectarrays for Ka-Band Applications,” IEEE Trans. Antenn. Propag., vol. 68, no. 8, pp. 6441–6446, Aug. 2020., doi:

[8] P. Xu, L. Li, R. Li, and H. Liu, “Dual-circularly polarized spin decoupled reflectarray with FSS-back for independent operating at Ku-/Ka-bands,” IEEE Trans. Antenn. Propag., vol. 69, no. 10, pp. 7041–7046, Oct. 2021. 10.1109/TAP.2021.3076518

[9] A. Samaiyar, M. Elmansouri, and D. S. Filipovic, “Shared-Aperture Reflectarrays and Antenna Arrays for In-Band Full-Duplex Systems,” IEEE Trans. Antenn. Propag., vol. 71, no. 11, pp. 9095–9100, Nov. 2023. 10.1109/TAP.2023.3309096

[10] X. Xuan, K. Wang, M. Deng, H. Wang, K. Fan, and J. Hu, “A Dual-Circularly Polarized Magneto-Electric Dipole Reflectarray With Independent Beam Control,” IEEE Antennas Wirel. Propag. Lett., vol. 23, no. 6, pp. 1824–1828, Jun. 2024., doi:

[11] [S. Gao, S. Li, H. Zhao, and X. Yin, “Compact dual-circularly polarized reflectarray antenna using semicircle strips elements with independent focus and beam directions,” IEEE Trans. Antenn. Propag., vol. 72, no. 5, pp. 4339–4348, May 2024. 10.1109/TAP.2024.3380739

[12] H.-X. Xu, T. Cai, Y.-Q. Zhuang, Q. Peng, G.-M. Wang, and J.-G. Liang, “Dual-Mode Transmissive Metasurface and Its Applications in Multibeam Transmitarray,” IEEE Trans. Antenn. Propag., vol. 65, no. 4, pp. 1797–1806, Apr. 2017., doi:

[13] W. Yang, K. Chen, J. Zhao, T. Jiang, and Y. Feng, “A Wideband High-Efficiency Transmit-Reflect-Array Antenna for Bidirectional Radiations With Distinct Circular Polarizations Based on a Metasurface,” IEEE Trans. Antenn. Propag., vol. 71, no. 4, pp. 3695–3700, Apr. 2023. 10.1109/TAP.2023.3249911

[14] C. Pan, H. Ren, K. Wang, J. F. Kolb, M. Elkashlan, M. Chen, et al., “Reconfigurable intelligent surfaces for 6G systems: Principles, applications, and research directions,” IEEE Commun. Mag., vol. 59, no. 6, pp. 14–20, Jun. 2021. 10.1109/MCOM.001.2001076

[15] B. Rana, S.-S. Cho, and I.-P. Hong, “Review Paper on Hardware of Reconfigurable Intelligent Surfaces,” IEEE Access, vol. 11, pp. 29614–29634, 2023. 10.1109/ACCESS.2023.3261547

[16] G. Oliveri, F. Zardi, P. Rocca, M. Salucci, and A. Massa, “Building a smart EM environment -AI-enhanced aperiodic micro-scale design of passive EM skins,” IEEE Trans. Antenn. Propag., vol. 70, no. 10, pp. 8757–8770, Oct. 2022. 10.1109/TAP.2022.3151354

[17] P. Callaghan and P. R. Young, “Investigation into Shaped Wide-Beam Reflectarray Surfaces Reflectors as Passive Repeaters in Wireless Networks,” J. Electron. Electr. Eng., vol. 4, no. 1, 2025., doi:

[18] R. Flamini, D. De Donno, J. Gambini, F. Giuppi, C. Mazzucco, A. Milani, et al., “Towards a heterogeneous smart electromagnetic environment for millimeter-wave communications: An industrial viewpoint,” IEEE Trans. Antenn. Propag., vol. 70, no. 10, pp. 8898–8910, Oct. 2022. 10.1109/TAP.2022.3151978

[19] P. Callaghan and P. R. Young, “Beam- and Band-Width Broadening of Intelligent Reflecting Surfaces Using Elliptical Phase Distribution,” IEEE Trans Antennas Prop., VOL. 70, NO. 10, pp 8825, Oct. 2022, doi:

[20] A. D. Olver, “Basic properties of antennas” in Handbook of Antenna Design, vol. 1. London: Peter Peregrinus Ltd, 1982, .

[21] R. Marks, Tables of Fourier Transform” in Handbook of Fourier Analysis & Its Applications Oxford University Press 2008 available at https://handbookoffourieranalysis.com/Files/Tables.pdf

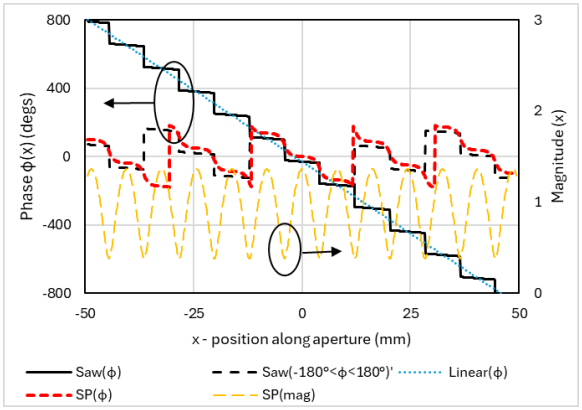
[22] L. Moustafa, R. Gillard, F. Peris, R. Loison, H. Legay, and E. Girard, “The Phoenix Cell: A New Reflectarray Cell With Large Bandwidth and Rebirth Capabilities,” IEEE Antennas Wirel. Propag. Lett., vol. 10, pp. 71–74, 2011., doi:

[23] P. Callaghan, P. Young, and C. Gu, “Corner reflectarray for indoor wireless applications,” in Proc. Antennas Propag. Conf. (APC), Birmingham, U.K., 2019, pp. 1–5.

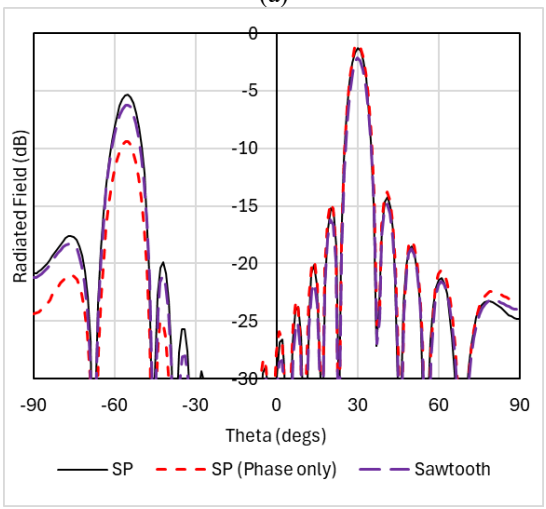
[24] L. Stark, “Microwave theory of phased-array antennas—A review,” Proc. IEEE, vol. 62, no. 12, pp. 1661–1701, Dec. 1974., doi: 10.1109/PROC.1974.9684

AWPL-01-26-0064

Figures (original graphics in *Callaxx* files)

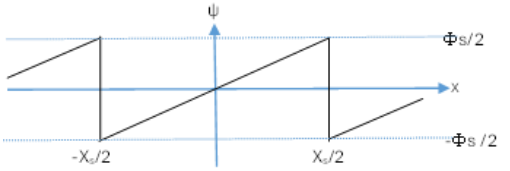


(a)

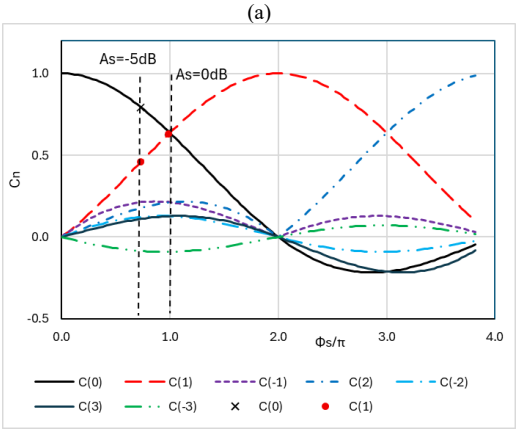


(b)

Fig. 1. Generation of dual-beam for an aperture 99 mm wide at 28 GHz θ_0=30°, θ_1=-55° that differ by 6 dB (a) phase and amplitude of fields with superposed waves compared to phases using 'sawtooth function' (b) resulting radiation patterns



(a)



(b)

Fig. 2. Fourier analysis of sawtooth phase function (a) definition of sawtooth parameters (b) plot of Fourier harmonic coefficients

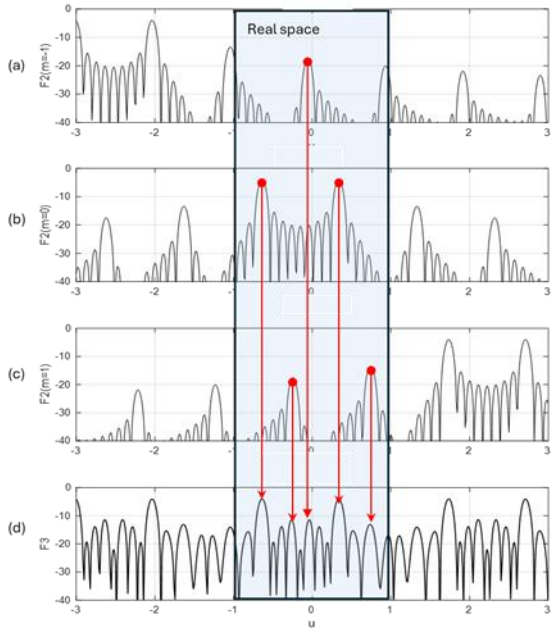


Fig. 3. $F_3(u)$ plotted against u (sin θ) for array of elements spaced d=4.5 mm at 28 GHz to give equal amplitude twin lobes at θ_0=20°, θ_1= - 40° constructed from Fourier elements (a) *m*=-1 (b) *m*=0 (c) *m*=1 (d) Sum of all components (here using 21 terms; *m*= -10 to +10)

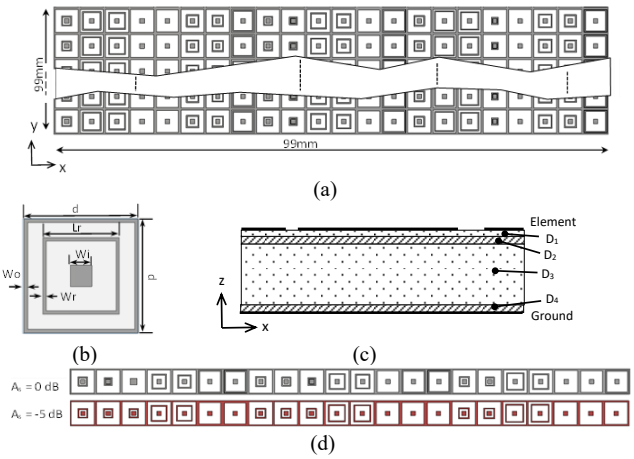


Fig. 4: Details of Prototype RAS
(a) Overall view (b) Details of Phoenix element d = 4.5mm, Wo = 0.2 mm, Wr = 0.2 mm, Wi = 0.8 (c) Profile of structure (d) comparison of designs for A_s = 0 dB and -5 dB

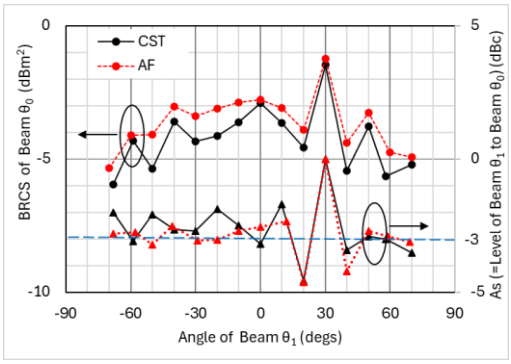


Fig. 6. Beam magnitudes in the x-z plane at 28 GHz, Ex. θ_0 fixed at 30° with a design target of A_s = -3 dB. Second beam, θ_1, varied -70° to +70°.

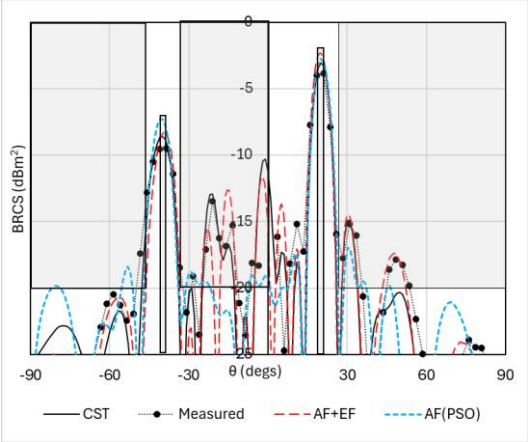


Fig. 5. Normalized (BRCS) patterns in the x-z plane for 'prototype' at 28 GHz, Ex with θ_0 = 20°, θ_1 = -40°, A_s = -5dB. Comparing CST simulation to measurement, AF (plus element Factor using equation (10) with n=m=-6…6) and AF further optimised using a PSO. Shaded areas indicate the template used for the PSO (desired pattern).